Front. Environ. Sci. Eng. 2021, 15(5): 107
https://doi.org/10.1007/s11783-021-1395-5

RESEARCH ARTICLE

Fabrication of magnetic multi-template molecularly imprinted polymer composite for the selective and efficient removal of tetracyclines from water

Guolong Zeng, Yiyang Liu, Xiaoguo Ma (✉), Yinming Fan

School of Environmental Science and Engineering, Guangdong University of Technology, Guangzhou 510006, China

HIGHLIGHTS

- Magnetic multi-template molecularly imprinted polymer composite was synthesized.
- MIP composite was used as the adsorbent for removal of tetracyclines from water.
- MIP composite showed excellent adsorption selectivity toward tetracyclines.
- MIP composite possessed good reusability.

GRAPHIC ABSTRACT

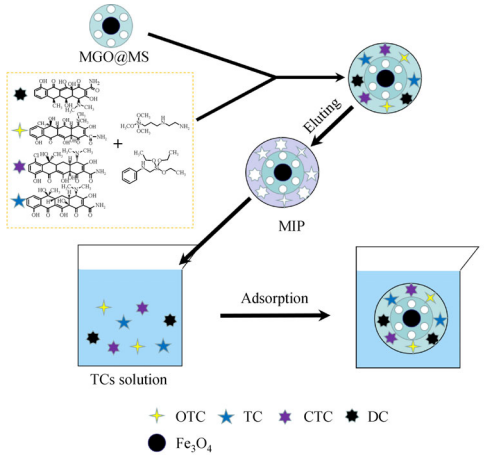

ARTICLE INFO

Article history:
Received 25 May 2020
Revised 4 December 2020
Accepted 7 December 2020
Available online 25 January 2021

Keywords:
Tetracyclines
Removal
Adsorption
Molecularly imprinted polymer
Magnetic graphene oxide

ABSTRACT

Antibiotic contamination of the water environment has attracted much attention from researchers because of their potential hazards to humans and ecosystems. In this study, a multi-template molecularly imprinted polymer (MIP) modified mesoporous silica coated magnetic graphene oxide (MGO@MS@MIP) was prepared by the surface imprinting method via a sol-gel process and was used for the selective, efficient and simultaneous removal of tetracyclines (TCs), including doxycycline (DC), tetracycline (TC), chlorotetracycline (CTC) and oxytetracycline (OTC) from water. The synthesized MIP composite was characterized by Fourier transform infrared spectroscopy, transmission electron microscope and thermogravimetric analysis. The adsorption properties of MGO@MS@MIP for these TCs were characterized through adsorption kinetics, isotherms and selectivity tests. The MIP composite revealed larger adsorption quantities, excellent selectivity and rapid kinetics for these four tetracyclines. The adsorption process was spontaneous and endothermic and followed the Freundlich isotherm model and the pseudo-second-order kinetic model. The MGO@MS@MIP could specifically recognize DC, TC, CTC and OTC in the presence of some chemical analogs. In addition, the sorption capacity of the MIP composite did not decrease significantly after repeated application for at least five cycles. Thus, the prepared magnetic MIP composite has great potential to contribute to the effective separation and removal of tetracyclines from water.

1 Introduction

Tetracyclines (TCs) can be used for the prevention and therapy of animal diseases. In China, TCs are the second most commonly applied antibiotics (Yang et al., 2013). Representative TCs including doxycycline (DC), tetracycline (TC), chlorotetracycline (CTC) and oxytetracycline (OTC) are widely used as feed additives for animal husbandry and veterinary drugs for their low cost and good

✉ Corresponding author
E-mail: xgma@21cn.com

properties (Lian et al., 2018). However, the excretion of animal waste with TCs and the discharge of wastewater from pharmaceutical factories and animal farms can lead to water pollution by TCs. The accumulation of TCs in the environment can create many health human hazards, such as antibiotic resistance, allergic reactions and gastrointestinal disorders (Tsai et al., 2009). Thus, the development of an efficient method for removing residual TCs in water from the environment is important.

Some methods for removing TC from water include adsorption (Ahmed, 2017), electrochemistry (Radjenovic and Petrovic, 2017), photodegradation (Zyoud et al., 2019) and biodegradation (Chen et al., 2018). However, limitations of electrochemistry, photodegradation and biodegradation during their use include their high energy consumption, poor light source conditions and antibiotic inhibition. Adsorption treatment is a simple and efficient method for removing TC, which involves the application of various sorbents, including magnetic carbon composites (Rattanachueskul et al., 2017), bio-char (Liu et al., 2012), magnetic resin (Zhou et al., 2012), rice husk ash (Chen et al., 2016), spent coffee grounds (Dai et al., 2019) and other substances. However, low adsorption capacity, long adsorption equilibrium time and poor adsorption selectivity restrict the practical applications of these adsorbents.

Molecular imprinting technology can selectively identify target substances in complex systems and can be used for substances that are difficult to separate and remove by traditional methods (Guo et al., 2018). Molecularly imprinted polymer (MIP) forms plenty of artificial recognition sites designed for target molecules during the synthesis process. These three-dimensional sites complement the target molecule in size, shape and functional groups and thus become highly selective adsorbent materials for target molecules (Cui et al., 2020). Nevertheless, some disadvantages of MIP synthesized by conventional methods include limited accessibility to imprinting sites, slow mass transfer rate, low recombination ability and incomplete template elimination (Li et al., 2018). For these reasons, surface molecular imprinting technology has received much attention during recent years for its high mass transfer efficiency, ease of removing template molecules and rapid sorption kinetics (Xu et al., 2011). However, the specific surface area of support materials has a great influence on the sorption capacity of surface MIP. Therefore, solid supports with large specific surface areas are required to improve the adsorption properties of MIP.

Graphene oxide (GO) is a two-dimensional carbon material with high specific surface area and rich oxygen-containing functional groups on its surface (Zhang et al., 2019). Thus, GO is considered an excellent carrier for synthesizing MIP and increasing the rebinding capacity, kinetic rate and water stability (Zhu et al., 2010; Ye et al., 2019). In general, centrifugation and filtration methods are used to separate the adsorbent material from aqueous solution (Duman et al., 2016). These applications are time-consuming and require extra costs (Duman et al., 2019). To improve separation efficiency, magnetic materials are introduced into adsorbents to allow convenient and rapid magnetic separation. Magnetic separation simplifies the separation process through the use of an external magnet (Xie et al., 2015; Wang et al., 2019). The combination of magnetic materials and GO can make up for the defects of GO during separation (Buelke et al., 2019; Liu et al., 2019). Mesoporous silica is known to have a large surface area and an easily modified surface, thus making it a suitable carrier for surface imprinting. Magnetic graphene oxide (MGO) coated with mesoporous silica not only prevents a loss of magnetism but also increases the surface area, which enhances the adsorption ability of MIP (Guo et al., 2019; Zhang et al., 2019).

In general, MIP is synthesized using a single compound as the template. Consequently, MIP cannot provide co-existing compounds with high affinity and selectivity during separation. In other words, a single-template MIP does not permit the simultaneous and effective removal of several components. To overcome this drawback, dual-template and multi-template MIP have recently emerged and have attracted much attention from researchers. Multi-template MIP has been shown to have superior specific recognition performance than single-template MIP (Ma et al., 2015). Multi-template MIP is thus a promising material with high practical application value. No studies to date have conducted molecular imprinting using multiple tetracyclines as templates.

In this study, a multi-template MIP using DC, TC, CTC and OTC as template molecules and N-[3-(trimethoxysilyl) propyl]ethylenediamine (KH-792) and anilinomethyl triethoxysilane (KH-42) as co-functional monomers was synthesized onto mesoporous silica modified magnetic graphene oxide (MGO@MS), and orthogonal optimization experiments were performed to optimize the synthesis conditions. The obtained MIP composite was characterized using a variety of techniques, and its adsorption properties, selectivity and reusability were investigated.

2 Materials and methods

2.1 Reagents and instruments

Doxycycline hyclate (DC), tetracycline hydrochloride (TC), chlorotetracycline hydrochloride (CTC), oxytetracycline hydrochloride (OTC), ciprofloxacin hydrochloride (CIP), methacycline (MTC), tetraethyl orthosilicate (TEOS), cetyltrimethylammonium bromide (CTAB), N-[3-(trimethoxysilyl)propyl]ethylenedi- amine (KH-792), anilinomethyl triethoxysilane (KH-42), graphite (325 meshes), methanol, acetonitrile and formic acid were purchased from Aladdin (Shanghai, China). Except for the reagents used in HPLC were of chromatographic grade,

other reagents were of analytical grade.

Fourier transform infrared (FT-IR) spectra were recorded by a Nicolet 380 spectrometer (Thermo Fisher Scientific, USA). The surface morphology of the products was observed by a Sigma HD (Zeiss, Germany) field emission scanning electron microscope (FE-SEM). Transmission electron microscopy (TEM) was conducted by a JEM-2100 microscope (JEOL, Japan). Surface area and pore structure were analyzed by a Brunauer-Emmett Teller (BET) apparatus (ASAP 2460, Micromeritics, USA).

Sample analysis was performed using an LC system containing an LC-20A solution system and a photodiode array detector (PDA) (Shimadzu, Japan). The analytes were separated on an inert Sustain C_{18} column (250 × 4.6 mm, 5 μm). The mobile phase consisted of methanol/acetonitrile/1% formic acid aqueous solution (1:2:7, V:V:V), the column temperature was kept constant at 35°C, and the flow rate was 1 mL/min. PDA detection was performed at 355 nm, and the injection volume was 10 μL.

2.2 Preparation of MGO@MS@MIP

Graphene oxide (GO), magnetic graphene oxide (MGO) and mesoporous silica modified magnetic graphene oxide (MGO@MS) were synthesized according to the procedures described in previous studies (Pourjavadi et al., 2015; Xie et al., 2019).

To improve the selectivity and adsorption properties of MGO@MS@MIP for DC, TC, CTC and OTC, surface molecular imprinting technology was used to prepare MIP. First, DC, TC, CTC and OTC (1 mmol, 1:1:1:1, molar ratio) were sonicated for 15 min so that they were fully dispersed in a 55-mL water/ethanol (1:10, v/v) mixture. After sonication, 1.4 mL of KH-792 and 0.6 mL of KH-42 were slowly added to the mixture, followed by churning for 2 h at 25°C. Next, 0.4 g of MGO@MS was added to the mixture and stirred vigorously for 24 h at room temperature. Finally, the solid product was subjected to cyclic elution using ethanol and glacial acetic acid (95:5, V:V) until no DC, TC, CTC and OTC were detected in the eluent by HPLC. Similarly, the non-imprinted polymer (NIP) composite was synthesized without the addition of these templates.

2.3 Adsorption experiments

The effects of solution pH, adsorption kinetics and isotherms of MGO@MS@MIP for TCs were studied. To test the effect of pH, a series of 20-mL solutions containing DC, TC, CTC and OTC (50 mg/L) were adjusted to different pH values (from 4 to 10) and then were mixed with the MIP composite (20 mg), followed by oscillation for 90 min at 298K and 150 r/min. The kinetic tests were conducted at specified intervals (from 1 to 360 min) at 298K and pH 7 with an initial concentration of 50 mg/L for each TC. Adsorption isotherm experiments were performed using different initial concentrations from 1 to 100 mg/L at pH 7 for 60 min. After achieving the sorption equilibrium and separating the mixture by an external magnetic field, the remaining liquid was filtered through a 0.22-μm membrane. HPLC was then used to determine the concentration of TCs in the filtered solution. The adsorption capacity was calculated using the following equation:

$$Q_e = (C_0 - C_e) \cdot V / m, \tag{1}$$

where Q_e (mg/g) stands for sorption quantity; C_0 and C_e (mg/L) are the initial concentration and equilibrium concentration, respectively; V (L) is the solution volume, and m (g) is the adsorbent amount.

2.4 Selectivity tests

To demonstrate the selectivity of MIP for DC, TC, CTC and OTC, two compounds with similar chemical structures to the templates, methacycline (MTC) and ciprofloxacin (CIP), were used as the competitive substances in the selectivity tests. Twenty mg MIP or NIP composite was added to 20 mL of mixed solution containing 50 mg/L of DC, TC, CTC, OTC, MTC and CIP. After being fully dispersed, the mixture was shaken at 298K and 150 r/min for 60 min to reach equilibrium. After magnetic separation, the residual concentrations of these compounds in the supernatant were measured. To better express the selectivity of MIP, the distribution coefficient (K_d), selectivity coefficient (α) and relative selection coefficient (β) were calculated as follows:

$$K_d = \frac{(C_0 - C_e) \cdot V}{C_e \cdot m}, \tag{2}$$

$$\alpha = \frac{K_{d1}}{K_{d2}}, \tag{3}$$

$$\beta = \frac{\alpha_{\mathrm{MIP}}}{\alpha_{\mathrm{NIP}}}, \tag{4}$$

where K_{d1} and K_{d2} are the distribution coefficients for a template and a competitive compound, respectively.

2.5 Regeneration experiments

Twenty mg of MIP composite was added to 20 mL of TCs mixture solution at a concentration of 50 mg/L. When the adsorption was balanced, the mixture was magnetically separated, and the remaining solution was detected by HPLC. A mixture of methanol and glacial acetic acid (9:1, V:V) was used to repeatedly elute the used MIP composite to completely remove the template molecules from the composite. Finally, the regenerated MIP composite was washed with methanol and dried in vacuum for later use.

The MIP composite was subjected to the above procedures several times to explore its reusability.

3 Results and discussion

3.1 Preparation of the MIP composite

The synthesis of MIP composite is shown in Fig. 1. Initially, magnetic Fe_3O_4 particles were introduced on the surface of GO via the chemical coprecipitation method. Subsequently, the magnetic GO (MGO) was covered by a silicon layer (MGO@MS) through the hydrolysis reaction of TEOS and the removal of CTAB to obtain a high specific surface area. In the preparation of MIP, template molecules (DC, TC, CTC and OTC) and functional monomers (KH-792 and KH-42) were first subjected to a prepolymerization process in a mixture of ethanol and water. MGO@MS was then added as the carrier of the prepolymerized mixture. The imprinted polymer obtained after elution had several specific imprinting sites, which resulted in its selectivity for the recognition of the template molecules. To optimize the synthesis conditions, the amounts of MGO@MS and functional monomers were modulated by conducting orthogonal experiments. The results (Table S1) indicated that when 0.4 g of MGO@MS was used as the supporting material and 1.4 mL of KH-792 and 0.6 mL of KH-42 as the co-functional monomers, the synthesized MIP composite had the highest adsorption capacity for the TCs. Hence, these quantities were used to prepare the MIP composite.

3.2 Characterization of MIP composite

The morphology of MGO, MGO @MS and MGO @MS @MIP was analyzed using TEM. Many solid particles—Fe_3O_4 crystals—could be observed in Fig. 2(a). Figure 2(b) shows the pore structure. However, because of the irregularity of the pore structure and the influence of triiron tetroxide, the pore structure was not clear in this figure. In Fig. 2(c), the roughness of MGO@MS@MIP virtually disappeared, which was caused by the filling of the holes with imprinted polymer, indicating that the imprinted polymer had been successfully modified on the

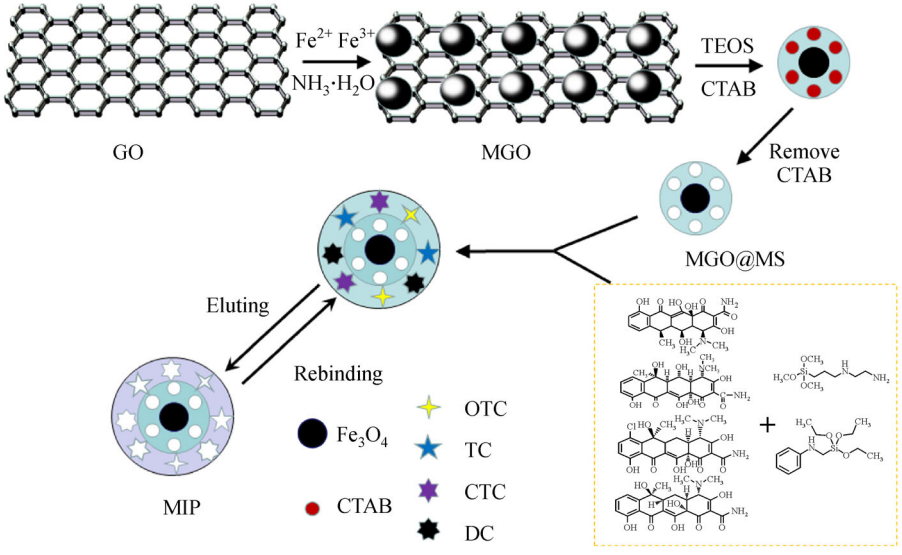

Fig. 1 Schematic diagram of the synthesis of MGO@MS@MIP.

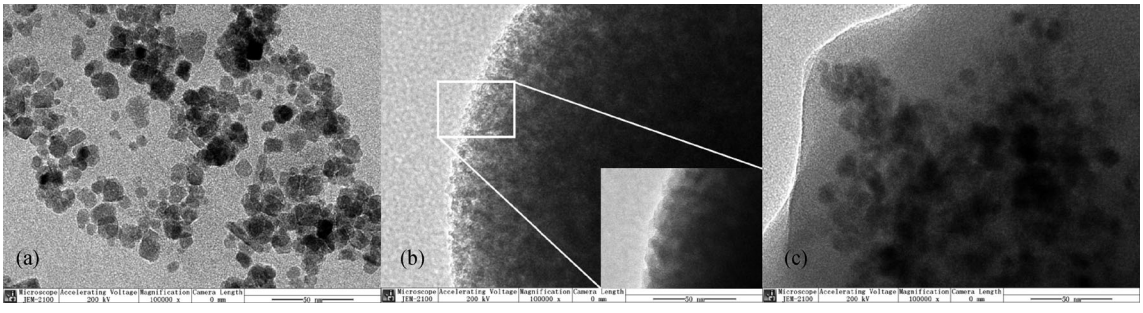

Fig. 2 TEM images of MGO (a), MGO@MS (b) and MGO@MS@MIP (c).

matrix material.

The mesoporous structures of MGO@MS and MGO@MS@MIP were verified by a BET N_2 adsorption/desorption test. MGO@MS displayed the type IV isotherm with a H4-type hysteresis loop in the relative pressure (p/p_0) range of 0.45–1.0, which is a typical characteristic of mesoporous structures (Fig. 3(a)). The specific surface area, pore size and pore volume of the MGO@MS were 480.642 m^2/g, 2.614 nm and 0.314 cm^3/g, respectively. In Fig. 3(b), MGO@MS@MIP also displayed a type IV isotherm with a H4-type hysteresis loop, indicating that the imprinted composite still had a mesoporous structure. The synthesized imprinted materials had a mixed microporous and mesoporous pore structure from the change in the adsorption amount of the adsorption branch at low relative pressure, and a step in the desorption branch at the relative pressure (p/p_0) was 0.45 (Van Der Voort et al., 2002). The specific surface area, pore size and pore volume of the MGO@MS@MIP were 121.526 m^2/g, 2.134 nm and 0.687 cm^3/g, respectively. These results showed that a mesoporous silica layer was loaded onto MGO, and the imprinting layer was modified onto MGO@MS.

FT-IR was used to analyze the functional groups of related materials. Figure 4 shows the FT-IR spectra of GO (a), MGO (b), MGO@MS (c), MGO@MS@MIP (d) and MGO@MS@NIP (e). The absorption peaks at 3367, 1727, 1631 and 1229 cm^{-1} in curve (a) were attributed to-OH, C = O, C = C and C-O, respectively, indicating that GO had been successfully synthesized (Wang et al., 2010; Wang and Wei, 2017). However, the absorption peak of the C = O stretching vibration nearly disappeared, while the absorption band of Fe-O at 594 cm^{-1} appeared in curve (b), which was attributed to the loading of Fe_3O_4 particles on GO (Wei et al., 2016). The strong and wide absorption peak at 1089 cm^{-1} in curve (c) was from the stretching vibration of Si-O-Si, indicating that mesoporous silica was coated on the surface of MGO (Wang et al., 2014). The absorption band at approximately 3440 cm^{-1} in curves (d) and (e) belonged to the N-H bending vibration of the functional monomers (Zhang et al., 2020). Curves (d) and (e) had similar vibrational absorption peaks, revealing that MIP and NIP had similar structures and chemical bonds and that the template molecules were completely removed during imprinting material synthesis. The above results indicated that all of the materials at the corresponding steps were successfully prepared.

Figure 5 shows the TGA results of MGO, MGO@MS and MGO@MS@MIP from 25°C to 900°C under a nitrogen atmosphere. The curves of the three materials revealed a decrease in mass at temperatures between 30°C and 130°C because of the desorption of physically adsorbed water (Kallenberger and Froba, 2018). The small mass loss of MGO and MGO@MS at 200°C–400°C likely stems from the decomposition of oxygen-containing functional groups on the surface of graphene oxide. An obvious slope change at 400°C–600°C was observed, which was caused by the decomposition of the GO skeleton. The mass loss of MGO@MS@MIP

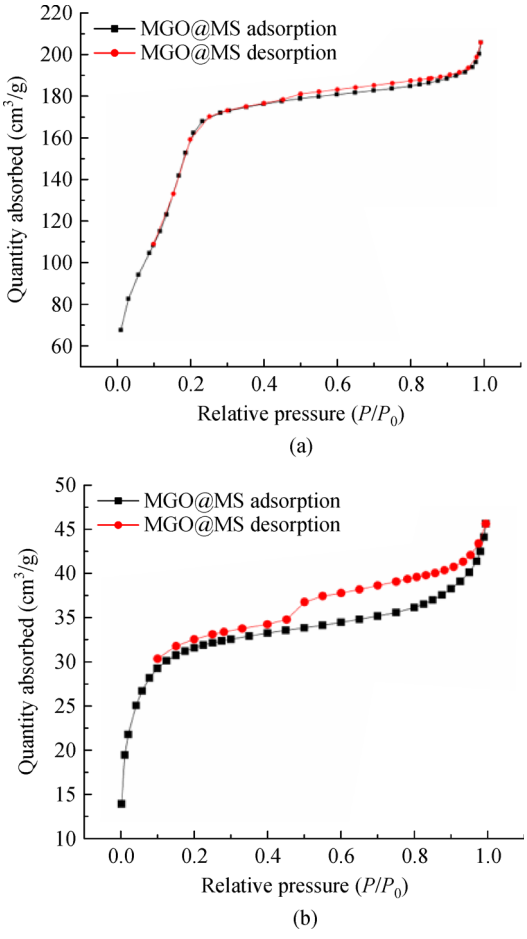

Fig. 3 N_2 adsorption-desorption isotherms of MGO@MS (a) and MGO@MS@MIP (b).

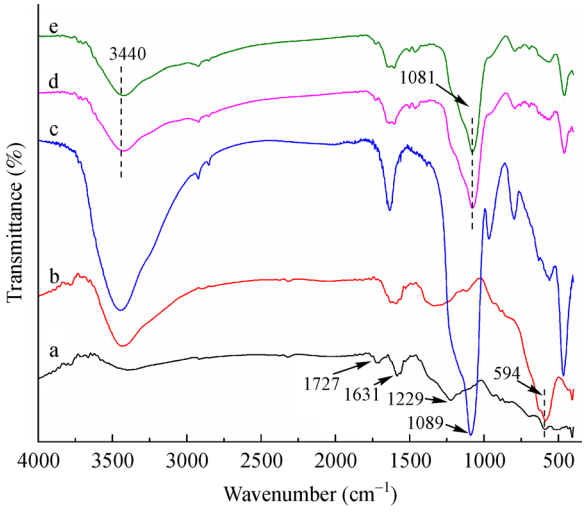

Fig. 4 FTIR spectra of GO (a), MGO (b), MGO@MS (c), MGO@MS@MIP (d) and NIP (e).

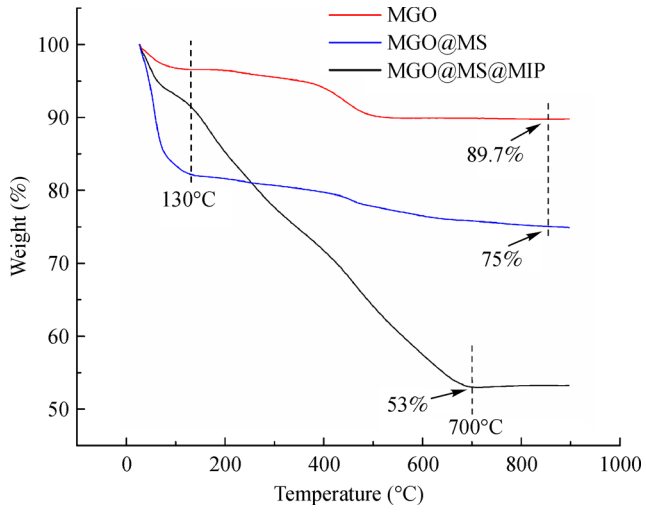

Fig. 5 TGA curves of MGO, MGO@MS and MGO@MS@-MIP.

primarily stemmed from the gradual decomposition of the imprinted layer when the temperature was above 200°C and stabilized to 53% of the mass after 700°C (Guardia et al., 2012).

3.3 Adsorption study

3.3.1 Effect of pH

The pH of the solution may affect the functional groups on the adsorbent surface and the species distribution of adsorbate in solution. As shown in Fig. 6, the maximum adsorption capacities of MIP for OTC, TC were achieved at pH 8 and for CTC, DC at pH 7.5 (Fig. 6). Because CTC is easily hydrolyzed under strongly alkaline conditions, the maximum pH for CTC adsorption was maintained at 8.5 (Kang et al., 2012; Xu et al., 2018). Under acidic conditions, the adsorption of TCs on the MIP composite was lower because H^+ combined with the amino group on the surface of MIP to form-NH_3^+, which caused a decrease in the MIP adsorption for TC. As the pH increased, the effect of H^+ decreased, thus enhancing the adsorption capacity. As the pH continued to increase, the adsorption amount decreased and was especially low at pH 10. This observation might be explained by the fact that the pKa of TCs is between 3.2 and 9.6 (Du et al., 2019); consequently, hydroxide ion in the solution may affect the speciation of TCs in water, resulting in a decrease in adsorption capacity.

3.3.2 Adsorption kinetics

Adsorption kinetics can reveal changes in the adsorption capacity of a sorbent with contact time. The adsorption kinetics of the four TCs on the MGO@MS@MIP is shown in Fig. 7. Because of the several empty binding sites on the surface of the MIP composite, the adsorption amounts of DC, TC, CTC and OTC increased rapidly within 20 min, and adsorption equilibrium was reached after 60 min. The rapid kinetics of the MIP composite for the TCs was attributed to the surface imprinting effect. Because the imprinting sites were distributed on the surface of the composite, the TC molecules in solution were able to easily access these imprinting sites. Consequently, adsorption could reach equilibrium more rapidly. To investigate the dynamic mechanism, the adsorption data were fitted by the pseudo-first-order kinetic model, pseudo-second-order

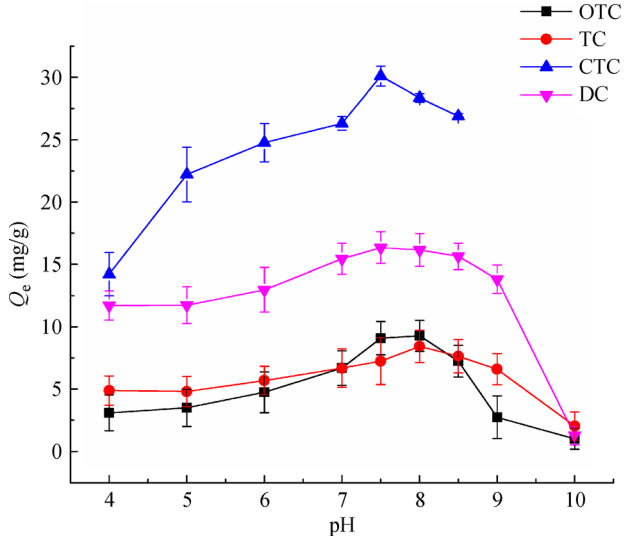

Fig. 6 Effect of sample pH on the adsorption of OTC, TC, CTC and DC by MGO @MS@MIP. Adsorption conditions: 20 mL of adsorbate solution (50 mg/L); 20 mg of adsorbent; 90 min of contact time; and 298 K.

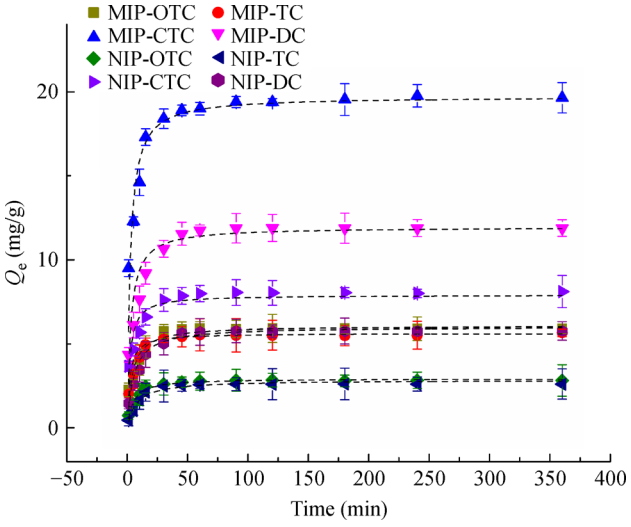

Fig. 7 Adsorption kinetic curves of OTC, TC, CTC and DC on MGO@MS@MIP and NIP. Adsorption conditions: 20 mL of adsorbate solution (50 mg/L); 20 mg of adsorbent; pH 7.5; and 298K.

kinetic model and intra-particle diffusion model (Xie et al., 2019), which were respectively expressed as:

$$\ln(Q_e - Q_t) = \ln Q_e - k_1 t, \tag{5}$$

$$t/Q_t = 1/k_2 Q_e^2 + t/Q_e, \tag{6}$$

$$Q_t = k_p t^{1/2} + C, \tag{7}$$

where Q_t (mg/g) is the adsorption amount of each TC at time t (min); Q_e (mg/g) is the equilibrium adsorption amount of each TC; k_1 (min^{-1}) and k_2 (mg/g/min) indicate the pseudo-first-order rate constant and the pseudo-secondary rate constant, respectively; C (mg/g) is the intercept; and k_p (mg/(g·$min^{1/2}$)) represents the intra-particle diffusion rate constant.

The corresponding kinetic parameters for the fitted graphs of the three dynamic models at 298K are shown in Supporting Information Fig. S1 and Table 1. The pseudo-second-order kinetic model most accurately described the MIP adsorption process of the selected TCs with the highest regression value (R^2) up to 0.9998, suggesting that chemical interactions may be related to the adsorption process. Similar results were obtained for the adsorption kinetics of other pollutants onto different adsorbents (Duman and Ayranci, 2010; Duman et al., 2015).

3.3.3 Adsorption isotherms

The study of isotherms can reveal the mechanism underlying the interaction between adsorbent and adsorbate. The adsorption isotherms of MGO@MS@MIP for the TCs were studied at 298K, 308K and 318K. As the initial concentrations of DC, TC, CTC and OTC increased, the adsorption capacities first increased rapidly and then gradually became saturated (Fig. 8). The obtained adsorption data were fitted to the Langmuir model and the Freundlich and Tempkin models (Xie et al., 2019), which can be respectively expressed as:

$$C_e/Q_e = C_e/Q_m + 1/K_L Q_m, \tag{8}$$

$$\ln Q_e = \ln K_F + \ln C_e/n, \tag{9}$$

$$Q_e = a + b\ln C_e, \tag{10}$$

where Q_m (mg/g) is the maximum adsorption quantity; Q_e (mg/g) is the equilibrium adsorption quantity; C_e (mg/L) represents the equilibrium concentration of TCs; K_L (L/mg) and K_F are the binding coefficients for the Langmuir model and Freundlich model, respectively; and a, b and n are constants.

Supporting Information Figs. S2–S5 and Table 2 presented the model fitting graphs and their corresponding parameters. Table 2 reveals that the MIP composite had a larger adsorption quantity, which stemmed from the large surface area of GO, and the imprinted polymer was synthesized on the surface of GO. Comparison of the correlation coefficients of the various models revealed that the Freundlich model best fit the adsorption process. The adsorption on the imprinted material was non-uniform and multi-layered, and the interaction between the adsorbates affected the isothermal adsorption behavior.

Figure S6 showed the chromatograms of a mixed solution containing 20 mg/L of DC, TC, CTC and OTC, before and after treatment by 20 mg of MIP for 60 min.

3.3.4 Adsorption thermodynamics

The relationship between the adsorption performance of the MIP composite and temperature was studied. A larger adsorption quantity was achieved at a higher temperature (Fig. 8). The adsorption thermodynamic behavior was assessed using the following equations:

$$\Delta G^0 = -RT\ln Q_e/C_e, \tag{11}$$

$$\Delta G^0 = \Delta H^0 - T\Delta S^0, \tag{12}$$

where T (K) is the temperature in Kelvin; R (8.314 J/(mol·K)) is the general gas constant; and ΔG^0 (kJ/mol), ΔH^0 (J/mol) and ΔS^0 (J/(mol·K)) are the Gibbs free energy change, standard enthalpy change and entropy change,

Table 1 Kinetic parameters of OTC, TC, CTC and DC adsorption onto the MGO@MS@MIP and NIP at 298K

Adsorbate	Adsorbent	$Q_{e,\,exp}$ (mg/g)	Pseudo-first order model			Pseudo-second order model			Intra-particle diffusion model		
			K_1 (/min)	$Q_{e,\,cal}$ (mg/g)	R^2	K_2 (mg/(g·min))	$Q_{e,cal}$ (mg/g)	R^2	K_{id} (mg/(g·$min^{1/2}$))	C (mg/g)	R^2
OTC	MIP	5.92	0.069	4.07	0.9426	0.043	6.42	0.9991	0.178	3.67	0.7232
	NIP	2.84	0.055	1.56	0.9280	0.078	2.85	0.9998	0.087	1.69	0.4568
TC	MIP	5.66	0.074	3.94	0.9556	0.091	5.84	0.9999	0.161	3.62	0.5128
	NIP	2.61	0.066	1.76	0.9322	0.047	2.64	0.9996	0.093	1.39	0.4620
CTC	MIP	19.76	0.068	13.30	0.9390	0.021	19.83	0.9999	0.452	13.60	0.5231
	NIP	8.10	0.068	5.55	0.9407	0.062	8.15	0.9999	0.207	5.32	0.5287
DC	MIP	11.89	0.069	8.18	0.9416	0.028	12.42	0.9998	0.372	7.25	0.5850
	NIP	5.76	0.072	4.66	0.9795	0.032	5.85	0.9996	0.202	3.10	0.5377

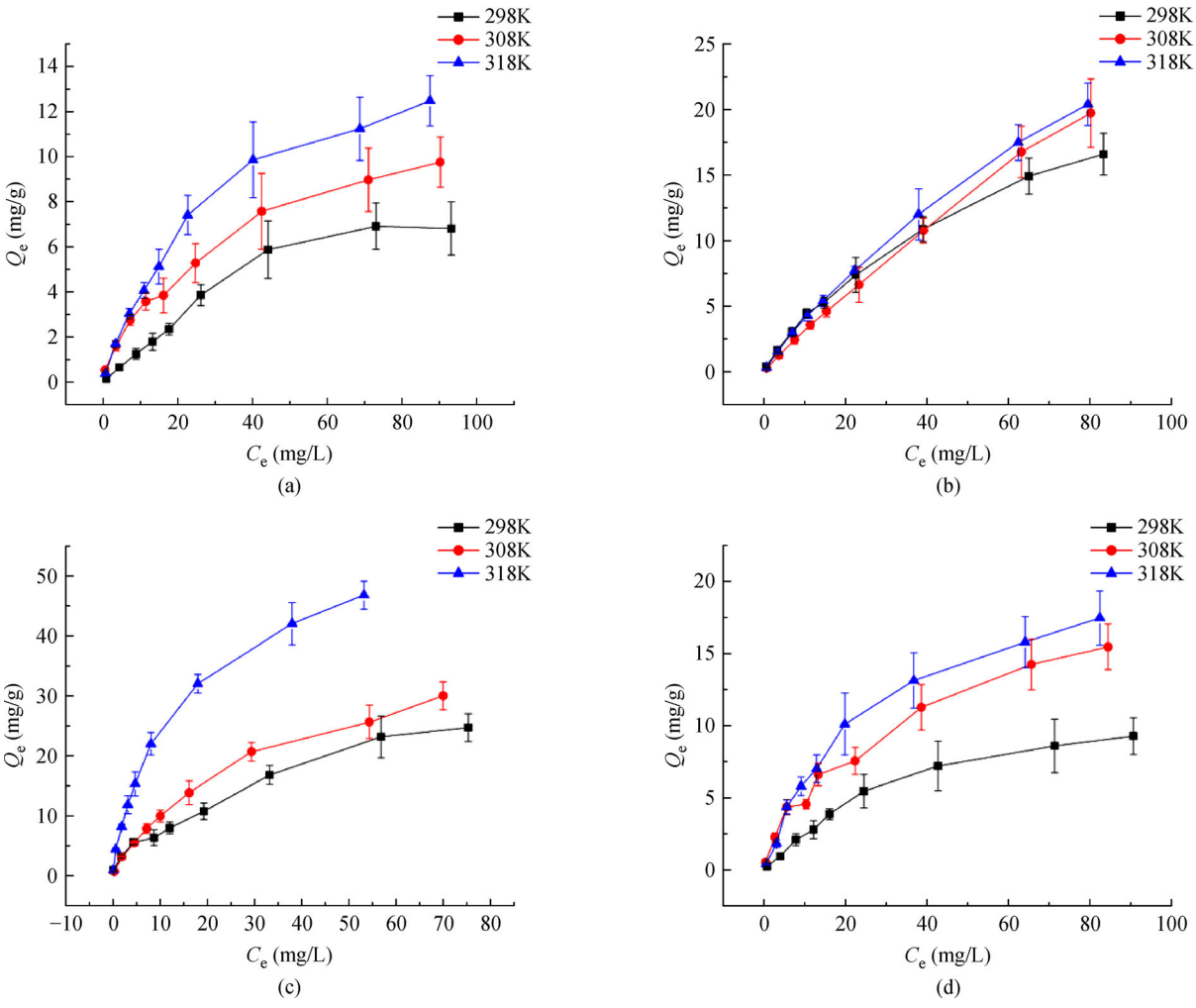

Fig. 8 Adsorption isotherms of MGO@MS@MIP for OTC (a), TC (b), CTC (c) and DC (d).

respectively.

Figure S7 and Table 3 show the thermodynamic graphs and their corresponding parameters, respectively. These fitting results indicate that the adsorption process was spontaneous, endothermic and dominated by physical adsorption.

3.3.5 Adsorption selectivity

Some compounds that are structurally similar to DC, TC, CTC and OTC may coexist in actual samples and thus can also be adsorbed by the MIP composite. For this reason, two structural analogs, methacycline (MTC) and ciprofloxacin hydrochloride (CIP), were used as competitive substances to examine adsorption selectivity. The allocation coefficients of DC, TC, CTC and OTC on the MIP composite were much larger than those of MTC and CIP (Table 4). Meanwhile, the selectivity coefficients of NIP were much lower than those of MIP. The above results indicated that the MIP composite possessed high sorption selectivity toward the TC templates, and a significant imprinting effect was achieved.

3.3.6 Regeneration and stability

To test the stability and reusability of the MIP composite, adsorption-desorption procedures were repeatedly conducted. The results of the re-use of the MIP composite indicated that the adsorption capacities of TCs decreased gradually (Fig. 9). However, even after five adsorption-elution cycles, the adsorption capacity of MGO@MS@MIP for DC, TC, CTC and OTC only decreased by 6.5%, 5.2%, 10.0% and 4.5% respectively. Thus, the MIP composite had high stability and reusability.

3.3.7 Comparison with other adsorbents

To demonstrate the advantages of the prepared MIP composite, the adsorption capacity and equilibrium time were compared with those of other reported adsorbents.

Table 2 Isotherm parameters of OTC, TC, CTC and DC adsorption onto MGO@MS@MIP at different temperatures

Adsorbate	Adsorbent	T (K)	Langmuir			Freundlich			Tempkin		
			Q_m (mg/g)	K_L (L/mg)	R^2	K_F	n (g/L)	R^2	a (mg/g)	b (L/g)	R^2
OTC	MIP	298	8.19	0.082	0.9613	0.18	2.14	0.9896	0.78	1.24	0.8976
		308	38.02	0.004	0.9305	0.84	1.09	0.9993	−1.93	2.02	0.7242
		318	18.80	0.031	0.9897	0.68	1.42	0.9737	−0.64	2.62	0.8822
	NIP	298	23.04	0.009	0.8110	0.17	1.05	0.9578	−1.83	2.14	0.7613
		308	4.62	0.16	0.8917	0.45	1.68	0.8169	0.28	1.01	0.6053
		318	35.72	0.010	0.5293	0.44	1.20	0.9461	−3.21	3.21	0.7566
TC	MIP	298	31.45	0.017	0.9696	0.64	1.30	0.9930	−1.56	3.40	0.8072
		308	95.20	0.004	0.9021	0.36	1.08	0.9994	−2.93	3.99	0.7472
		318	57.80	0.008	0.9895	0.50	1.15	0.9960	−2.81	4.21	0.7608
	NIP	298	35.58	0.011	0.8030	0.16	0.87	0.8650	−2.94	3.57	0.8022
		308	17.69	0.038	0.8199	0.65	1.36	0.9190	−0.98	2.86	0.8036
		318	62.50	0.014	0.7729	0.95	1.20	0.9430	−1.91	5.55	0.8244
CTC	MIP	298	39.84	0.039	0.8560	2.92	2.16	0.9702	4.36	3.22	0.6406
		308	54.05	0.033	0.9564	1.92	1.47	0.9912	1.20	5.44	0.8186
		318	98.04	0.12	0.9790	5.43	1.67	0.9828	9.95	7.36	0.8361
	NIP	298	15.38	0.13	0.9460	1.44	2.74	0.9250	0.54	2.62	0.8651
		308	31.35	2.85	0.9380	1.50	2.46	0.9100	2.92	4.87	0.8858
		318	192.31	26.0	0.6560	1.53	2.34	0.9122	17.4	9.61	0.6495
DC	MIP	298	22.34	0.040	0.9750	0.34	1.57	0.9676	0.07	3.00	0.8352
		308	13.69	0.039	0.9531	1.09	1.34	0.9845	−0.99	3.12	0.7706
		318	9.22	0.032	0.9790	0.65	1.21	0.9955	−0.65	1.64	0.4783
	NIP	298	44.82	0.011	0.5600	0.76	1.38	0.9799	−1.59	3.68	0.6969
		308	24.80	0.024	0.7768	0.76	1.41	0.9545	−1.24	3.42	0.8227
		318	21.85	0.10	0.9846	1.51	1.33	0.9720	1.80	3.38	0.8186

Table 3 Thermodynamic parameters of OTC, TC, CTC and DC adsorption onto the MGO @MS @MIP at various initial concentrations and temperatures

Adsorbate	C_0 (mg/L)	H^0 (J/mol)	S^0 (J/(mol·K))	G^0 (kJ/mol)		
				298K	308K	318K
OTC	10	50.12	2.22	−0.61	−0.63	−0.65
	50	43.70	1.81	−0.49	−0.51	−0.53
	100	26.39	0.97	−0.26	−0.27	−0.28
TC	10	11.53	0.42	−0.114	−0.119	−0.123
	50	5.66	0.12	−0.029	−0.030	−0.031
	100	10.10	0.30	−0.079	−0.082	−0.085
CTC	10	49.36	2.41	−0.67	−0.69	−0.72
	50	33.78	1.55	−0.43	−0.44	−0.46
	100	38.63	1.73	−0.48	−0.49	−0.51
DC	10	41.92	1.87	−0.52	−0.53	−0.55
	50	28.82	1.17	−0.32	−0.33	−0.34
	100	37.80	1.51	−0.41	−0.43	−0.44

Table 4 Special selectivity of MIP composite toward TCs compared with MTC and CIP

Adsorbent	Imprinting parameter	OTC	TC	CTC	DC	CIP	MTC
MIPs	K_d	0.068	0.05	0.356	0.039	0.005	0.003
	α_{MTC}	12.53	9.22	65.64	7.13	–	–
	α_{CIP}	21.16	15.58	110.8	12.04	–	–
NIPs	K_d	0.009	0.007	0.026	0.006	0.004	0.004
	α_{MTC}	2.26	1.17	6.55	1.48	–	–
	α_{CIP}	2.26	1.17	6.55	1.48	–	–

Notes: Relative selection coefficient, β_{MTC} of OTC, TC, CTC, and DC are 5.54, 7.88, 13.32, and 4.81, respectively; β_{CIP} of OTC, TC, CTC, and DC are 9.36, 13.32, 16.92, and 8.14, respectively.

Table 5 Comparison with other sorbents for the removal of tetracyclines

Adsorbent	Q_e (mg/g)	Equilibrium time (h)	Reference
Magnetic carbon	28.14	5	Rattanachueskul et al., 2017
[a] Fe_3O_4/PAN NFs	37.17	72	Liu et al., 2015
[b] Magnetic PI@LDO	50.82	3	Wu et al., 2019
[c] Fe-N, N-SBA15	40.24	6	Zhang et al., 2015
MGO@MS@MIP	40.09	1	This work

Notes: a) Fe_3O_4/polyacrylonitrile (PAN) composite nanofibers (NFs). b) Core-shell structured magnetic polyimide@layered double oxides (LDO) composites. c) Sorbent made by grafting both amino groups and Fe (III) on mesoporous silica SBA15.

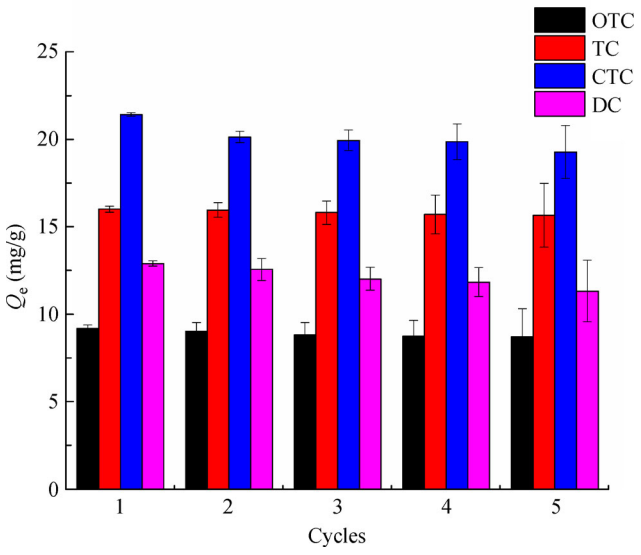

Fig. 9 The reusability analysis of MGO@MS@MIP for four TCs.

Magnetic PI@LDO composite had a higher sorption capacity than the MIP composite synthesized in this study, but its equilibrium time was much longer (3 h) than that of the latter (1 h) (Table 5). In addition, the MIP composite had much higher selectivity for TCs, which is beneficial for practical applications. Generally, the prepared MGO@MS@MIP adsorbent possessed high binding capacity, fast adsorption kinetics and good adsorption selectivity; thus, MGO@MS@MIP adsorbent has great potential to be used in the removal of TC contaminants from water.

4 Conclusions

A novel sorbent, multi-template molecularly imprinted polymer composite (MGO@MS@MIP), was synthesized and characterized in this study. Experimental results revealed that the MIP composite had good adsorption behavior for DC, TC, CTC and OTC in terms of capacity, selectivity, rapidity and reusability. The MIP composite had a special ability to reorganize itself toward TCs in complex systems because of the imprinting effect and could be rapidly and easily separated from aqueous solution using a magnet. Thus, MGO@MS@MIP might have excellent potential to be applied in the adsorption treatment of TCs in aqueous solution.

Acknowledgements This work was supported by the Science and Technology Planning Project of Guangzhou, China (No. 201803030040), the National Natural Science Foundation of China (Grant No. 41272262) and the Major Projects (Natural Science) of Education Department of Guangdong Province, China (261555101).

Electronic Supplementary material Supplementary material is available in the online version of this article at https://doi.org/10.1007/s11783-021-1395-5 and is accessible for authorized users.

References

Ahmed M J (2017). Adsorption of quinolone, tetracycline, and penicillin antibiotics from aqueous solution using activated carbons. Environmental Toxicology and Pharmacology, 50: 1–10

Buelke C, Alshami A, Casler J, Lin Y, Hickner M, Aljundi I H (2019). Evaluating graphene oxide and holey graphene oxide membrane

performance for water purification. Journal of Membrane Science, 588: 117195 doi:10.1016/j.memsci.2019.117195

Chen H Y, Liu Y D, Dong B (2018). Biodegradation of tetracycline antibiotics in A/O moving-bed biofilm reactor systems. Bioprocess and Biosystems Engineering, 41(1): 47–56

Chen Y J, Wang F H, Duan L C, Yang H, Gao J (2016). Tetracycline adsorption onto rice husk ash, an agricultural waste: Its kinetic and thermodynamic studies. Journal of Molecular Liquids, 222: 487–494

Cui Y, Tan F, Wang Y, Ren S, Chen J (2020). Diffusive gradients in thin films using molecularly imprinted polymer binding gels for in situ measurements of antibiotics in urban wastewaters. Frontiers of Environmental Science & Engineering, 14(6): 111

Dai Y J, Zhang K X, Meng X B, Li J J, Guan X T, Sun Q Y, Sun Y, Wang W S, Lin M, Liu M, Yang S S, Chen Y J, Gao F, Zhang X, Liu Z H (2019). New use for spent coffee ground as an adsorbent for tetracycline removal in water. Chemosphere, 215: 163–172

Du F Y, Sun L S, Tan W, Wei Z Y, Nie H G, Huang Z J, Ruan G H, Li J P (2019). Magnetic stir cake sorptive extraction of trace tetracycline antibiotics in food samples: preparation of metal-organic framework-embedded polyHIPE monolithic composites, validation and application. Analytical and Bioanalytical Chemistry, 411(10): 2239–2248

Duman O, Ayranci E (2010). Attachment of benzo-crown ethers onto activated carbon cloth to enhance the removal of chromium, cobalt and nickel ions from aqueous solutions by adsorption. Journal of Hazardous Materials, 176(1–3): 231–238

Duman O, Özcan C, Gürkan Polat T, Tunç S (2019). Carbon nanotube-based magnetic and non-magnetic adsorbents for the high-efficiency removal of diquat dibromide herbicide from water: OMWCNT, OMWCNT-Fe_3O_4 and OMWCNT-κ-carrageenan-Fe_3O_4 nanocomposites. Environmental Pollution, 244: 723–732

Duman O, Tunç S, Bozoğlan B K, Polat T G (2016). Removal of triphenylmethane and reactive azo dyes from aqueous solution by magnetic carbon nanotube-κ-carrageenan Fe_3O_4 nanocomposite. Journal of Alloys and Compounds, 687: 370–383

Duman O, Tunç S, Polat T G (2015). Determination of adsorptive properties of expanded vermiculite for the removal of C. I. Basic Red 9 from aqueous solution: Kinetic, isotherm and thermodynamic studies. Applied Clay Science, 109–110: 22–32

Guardia L, Suarez-Garcia F, Paredes J I, Solis-Fernandez P, Rozada R, Fernandez-Merino M J, Martinez-Alonso A, Tascon J M D (2012). Synthesis and characterization of graphene-mesoporous silica nanoparticle hybrids. Microporous and Mesoporous Materials, 160: 18–24

Guo J F, Yu M M, Wei X, Huang L H (2018). Preparation of core-shell magnetic molecularly imprinted polymer with uniform thin polymer layer for adsorption of dichlorophen. Journal of Chemical & Engineering Data, 63(8): 3068–3073

Guo L H, Ma X G, Xie X W, Huang R F, Zhang M Y, Li J, Zeng G L, Fan Y M (2019). Preparation of dual-dummy-template molecularly imprinted polymers coated magnetic graphene oxide for separation and enrichment of phthalate esters in water. Chemical Engineering Journal, 361: 245–255

Kallenberger P A, Froba M (2018). Water harvesting from air with a hygroscopic salt in a hydrogel-derived matrix. Communications Chemistry, 1(1): 28

Kang H J, Lim M Y, Kwon J H (2012). Effects of adsorption onto silica sand particles on the hydrolysis of tetracycline antibiotics. Journal of Environmental Monitoring, 14(7): 1853–1859

Li X, Ma X G, Huang R F, Xie X W, Guo L H, Zhang M Y (2018). Synthesis of a molecularly imprinted polymer on $mSiO_2@Fe_3O_4$ for the selective adsorption of atrazine. Journal of Separation Science, 41 (13): 2837–2845

Lian L L, Lv J Y, Wang X Y, Lou D W (2018). Magnetic solid-phase extraction of tetracyclines using ferrous oxide coated magnetic silica microspheres from water samples. Journal of Chromatography. A, 1534: 1–9

Liu H, Zhu J, Hao L, Jiang Y, Van Der Bruggen B, Sotto A, Gao C, Shen J (2019). Thermo- and pH-responsive graphene oxide membranes with tunable nanochannels for water gating and permeability of small molecules. Journal of Membrane Science, 587: 117163

Liu P, Liu W J, Jiang H, Chen J J, Li W W, Yu H Q (2012). Modification of bio-char derived from fast pyrolysis of biomass and its application in removal of tetracycline from aqueous solution. Bioresource Technology, 121: 235–240

Liu Q, Zhong L B, Zhao Q B, Frear C, Zheng Y M (2015). Synthesis of Fe_3O_4/polyacrylonitrile composite electrospun nanofiber mat for effective adsorption of tetracycline. ACS Applied Materials & Interfaces, 7(27): 14573–14583

Ma P F, Yang W M, Fan T, Liu H, Zhou Z P, Li J H, Zhang L, Xu W Z (2015). Surface imprinted polymers for oil denitrification with the combination of computational simulation and multi-template molecular imprinting. Polymers for Advanced Technologies, 26(5): 476–486

Pourjavadi A, Tehrani Z M, Salimi H, Banazadeh A, Abedini N (2015). Hydrogel nanocomposite based on chitosan-*g*-acrylic acid and modified nanosilica with high adsorption capacity for heavy metal ion removal. Iranian Polymer Journal, 24(9): 725–734

Radjenovic J, Petrovic M (2017). Removal of sulfamethoxazole by electrochemically activated sulfate: Implications of chloride addition. Journal of Hazardous Materials, 333: 242–249

Rattanachueskul N, Saning A, Kaowphong S, Chumha N, Chuenchom L (2017). Magnetic carbon composites with a hierarchical structure for adsorption of tetracycline, prepared from sugarcane bagasse via hydrothermal carbonization coupled with simple heat treatment process. Bioresource Technology, 226: 164–172

Tsai W H, Huang T C, Huang J J, Hsue Y H, Chuang H Y (2009). Dispersive solid-phase microextraction method for sample extraction in the analysis of four tetracyclines in water and milk samples by high-performance liquid chromatography with diode-array detection. Journal of Chromatography. A, 1216(12): 2263–2269

Van Der Voort P, Ravikovitch P I, De Jong K P, Neimark A V, Janssen A H, Benjelloun M, Van Bavel E, Cool P, Weckhuysen B M, Vansant E F (2002). Plugged hexagonal templated silica: a unique micro- and mesoporous composite material with internal silica nanocapsules. Chemical Communications, (9): 1010–1011

Wang J, Chen Z M, Chen B L (2014). Adsorption of polycyclic aromatic hydrocarbons by graphene and graphene oxide nanosheets. Environmental Science & Technology, 48(9): 4817–4825

Wang J J, Wei J (2017). Selective and simultaneous removal of dibenzothiophene and 4-methyldibenzothiophene using double-template molecularly imprinted polymers on the surface of magnetic mesoporous silica. Journal of Materials Chemistry. A, Materials for

Energy and Sustainability, 5(9): 4651–4659

Wang R, Ma X G, Zhang X J, Li X, Li D P, Dang Y F (2019). C8-modified magnetic graphene oxide based solid-phase extraction coupled with dispersive liquid-liquid microextraction for detection of trace phthalate acid esters in water samples. Ecotoxicology and Environmental Safety, 170: 789–795

Wang Z M, Wang W D, Coombs N, Soheilnia N, Ozin G A (2010). Graphene oxide-periodic mesoporous silica sandwich nanocomposites with vertically oriented channels. ACS Nano, 4(12): 7437–7450

Wei D, Li M T, Wang X D, Han F, Li L S, Guo J, Ai L J, Fang L L, Liu L, Du B, Wei Q (2016). Extracellular polymeric substances for Zn(II) binding during its sorption process onto aerobic granular sludge. Journal of Hazardous Materials, 301: 407–415

Wu H J, Zhang H L, Zhang W J, Yang X F, Zhou H, Pan Z Q, Wang D S (2019). Preparation of magnetic polyimide@ Mg-Fe layered double hydroxides core-shell composite for effective removal of various organic contaminants from aqueous solution. Chemosphere, 219: 66–75

Xie L W, Guo J F, Zhang Y P, Hu Y C, You Q P, Shi S Y (2015). Novel molecular imprinted polymers over magnetic mesoporous silica microspheres for selective and efficient determination of protocatechuic acid in *Syzygium aromaticum*. Food Chemistry, 178: 18–25

Xie X W, Ma X G, Guo L H, Fan Y M, Zeng G L, Zhang M Y, Li J (2019). Novel magnetic multi-templates molecularly imprinted polymer for selective and rapid removal and detection of alkylphenols in water. Chemical Engineering Journal, 357: 56–65

Xu S N, Ding J, Chen L G (2018). A fluorescent material for the detection of chlortetracycline based on molecularly imprinted silica-graphitic carbon nitride composite. Analytical and Bioanalytical Chemistry, 410(27): 7103–7112

Xu W Z, Zhou W, Xu P P, Pan J M, Wu X Y, Yan Y S (2011). A molecularly imprinted polymer based on TiO_2 as a sacrificial support for selective recognition of dibenzothiophene. Chemical Engineering Journal, 172(1): 191–198

Yang X Q, Yang C X, Yan X P (2013). Zeolite imidazolate framework-8 as sorbent for on-line solid-phase extraction coupled with high-performance liquid chromatography for the determination of tetracyclines in water and milk samples. Journal of Chromatography. A, 1304: 28–33

Ye B, Chen Z, Li X, Liu J, Wu Q, Yang C, Hu H, Wang R (2019). Inhibition of bromate formation by reduced graphene oxide supported cerium dioxide during ozonation of bromide-containing water. Frontiers of Environmental Science & Engineering, 13(6): 86

Zhang M Y, Ma X G, Li J, Huang R F, Guo L H, Zhang X F, Fan Y M, Xie X W, Zeng G L (2019). Enhanced removal of As(III) and As(V) from aqueous solution using ionic liquid-modified magnetic graphene oxide. Chemosphere, 234: 196–203

Zhang Y, Cheng X, Jiang X, Urban J J, Lau C H, Liu S, Shao L (2020). Robust natural nanocomposites realizing unprecedented ultrafast precise molecular separations. Materials Today, 36: 40–47

Zhang Z Y, Lan H C, Liu H J, Qu J H (2015). Removal of tetracycline antibiotics from aqueous solution by amino-Fe (III) functionalized SBA15. Colloids and Surfaces a-Physicochemical and Engineering Aspects, 471: 133–138

Zhou Q, Li Z Q, Shuang C D, Li A M, Zhang M C, Wang M Q (2012). Efficient removal of tetracycline by reusable magnetic microspheres with a high surface area. Chemical Engineering Journal, 210: 350–356

Zhu Y W, Murali S, Cai W W, Li X S, Suk J W, Potts J R, Ruoff R S (2010). Graphene and graphene oxide: Synthesis, properties, and applications. Advanced Materials, 22(35): 3906–3924

Zyoud A H, Zubi A, Zyoud S H, Hilal M H, Zyoud S, Qamhieh N, Hajamohideen A, Hilal H S (2019). Kaolin-supported ZnO nanoparticle catalysts in self-sensitized tetracycline photodegradation: Zero-point charge and pH effects. Applied Clay Science, 182: 105294